Journal of Nanoparticle Research (2005) 7: 203–208
DOI: 10.1007/s11051-004-7899-7
© Springer 2005

Synthesis of In_2O_3 nanoparticles by thermal decomposition of a citrate gel precursor

J.F.Q. Rey[1,2], T.S. Plivelic[2], R.A. Rocha[1], S.K. Tadokoro[1], I. Torriani[2,3] and E.N.S. Muccillo[1]
[1]*Centro Multidisciplinar para o Desenvolvimento de Materiais Cerâmicos, Instituto de Pesquisas Energéticase Nucleares – CCTM, C.P. 11049, S. Paulo 05422-970, SP, Brazil (Tel.: +55-11-38169343; Fax: +55-11-38169370; E-mail: enavarro@usp.br);* [2]*Laboratório Nacional de Luz Síncroton – LNLS, C.P. 6192, Campinas, SP, Brazil;* [3]*Instituto de Física Gleb Wataghin, UNICAMP, Campinas, SP, Brazil*

Received 1 September 2004; accepted in revised form 19 December 2004

Key words: Indium oxide, nanoparticles, thermal analysis, FTIR, TEM, SAXS, ceramics, sol-gel

Abstract

This paper describes the synthesis of indium oxide by a modified sol–gel method, and the study of thermal decomposition of the metal complex in air. The characterization of the intermediate as well as the final compounds was carried out by thermogravimetry, differential thermal analysis, Fourier transform infrared spectroscopy, X-ray diffraction, transmission electron microscopy, and small angle X-ray scattering. The results show that the indium complex decomposes to In_2O_3 with the formation of an intermediate compound. Nanoparticles of cubic In_2O_3 with crystallite sizes in the nanosize range were formed after calcination at temperatures up to 900°C. Calcined materials are characterized by a polydisperse distribution of spherical particles with sharp and smooth surfaces.

Introduction

Indium oxide (In_2O_3) has a C-type sesquioxide structure and is an n-type semiconductor with a wide band gap of about 3.6 eV. This material presents high transparency in the visible region and high electrical conductivity (Granqvist, 1993).

In_2O_3 has been widely used in optoelectronic devices such as solar cells and liquid crystal displays (Gopchandran et al., 1997). Moreover, it is an important material in the gas sensor field. Doped In_2O_3 gas sensors have high sensitivity to ozone and NO_x (Tadashi et al., 1993; Steffes et al., 2001; Tanaka & Esaka, 2001), and high sensitivity and selectivity to CO (Hiroyuki et al., 1997).

The synthesis of nanoparticles of either oxide and non-oxide materials has received great attention over the last two decades, since these materials are expected to exhibit special features that are distinct from those of microcrystalline materials or single crystals. The physical and chemical properties of these nanosized powders are influenced by shape, size and size distribution of the particles, which depend on the characteristics of synthesis (Matsumoto et al., 2001). For indium compounds, size-dependence of room temperature photoluminescence (Murali et al., 2001) and gas sensitivity (Gurlo et al., 1997) have been observed.

Nanoparticles of In_2O_3 have been synthesized by several techniques, such as controlled precipitation (Yura et al., 1990), forced hydrolysis (Hamada et al., 1993), sol–gel (Tahar et al., 1997; Perez-Maquela et al., 1998; Gurlo et al., 2003), sonohydrolysis (Avivi et al., 2000), reverse

microemulsion (Zhan et al., 2004), and mechanochemical processing (Yang et al., 2004). All these methods resulted in the production of indium hydroxide particles with different morphologies and sizes.

The synthesis of metal oxide particles by the sol–gel method using citric acid as a complexant agent is known for more than 30 years (Marcilly et al., 1970). It has been used to synthesize a number of ceramic materials to which the powder particles were in the nanosize range, and exhibited relatively high structural homogeneity (Hattori et al., 1993; Taguchi et al., 1997).

In this work an indium citrate gel was prepared by a modified sol–gel technique. The thermal decomposition of the metal complex in air and the characterization of intermediate and final product materials were carried out by several techniques. The main purpose of this work was to verify the possibility of using a relatively simple technique for the preparation of homogeneous nanoparticles of In_2O_3.

Experimental

Indium oxide (99.99%, Aldrich) and anhydrous citric acid were used as starting materials. Other reagents were of analytical grade. A stock solution of indium nitrate was prepared by dissolution of commercial indium oxide in a hot nitric acid solution. Another solution was prepared with citric acid and deionized water to act as a complexant agent.

The sol–gel technique used here involves the preparation of a solution containing one or more cations of interest, and adding to it a solution containing a complexant agent. The molar ratio metal:citric acid was 1:3.6. This molar ratio although arbitrary was suitably chosen to avoid precipitation. The solution was then heated up to 70°C under stirring to remove excess water and to convert it to a transparent gel. While rising the temperature, the solution became more viscous with the evolution of foam, and finally it gelled without any visible formation of precipitation or turbidity. This method of synthesis yields very fine and homogeneous nanoparticles. It involves the formation of weak hydrogen-bonded-like associates, in a non-rigid polymer network (Kakihana, 1996). The method used here is somewhat different from that originally proposed, in that the heating of the solution was interrupted before the formation of a resin-like material. The resulting citrate gel has a comparatively higher thermal stability.

The thermal decomposition behavior of the precursor material was studied by simultaneous thermogravimetry, TG, and differential thermal analysis, DTA (STA409, Netzsch). The precursor material (24 mg) was heated up to 1200°C with a heating rate of 5°C min^{-1} in flowing (50 ml min^{-1}) synthetic air. Alumina (Alumalux, Alcoa) was used as reference material. Fourier transform infrared spectroscopy, FTIR (Magna 560, Nicolet) study of the precursor gel and powders that have been calcined at various temperatures (150–700°C) was performed to gain more insight into the composition and structure of the precursor material, and to characterize the gel-to-powder conversion. This analysis was performed in transmission mode with a resolution of 4 cm^{-1} in the 4000–400 cm^{-1} wavenumber range. Specimens were prepared using the KBr method. The morphology of calcined nanoparticles was observed in a transmission electron microscope (JEM 200C, Jeol).

Powder diffraction of the thermally treated samples for phase characterization and lattice parameter determination were carried out in a diffractometer (Ultima II, Rigaku) using θ–θ configuration and Cu Kα radiation ($\lambda = 1.5405$ Å) from a Cu tube with graphite monochromator. The typical operating conditions were 40 kV and 35 mA. Scans were conducted at a sampling interval of 0.02° and counting time of 5 s in the 18–100° 2θ range. The lattice parameter was calculated using the celref software. The average crystallite size (d_{hkl}) of powder materials calcined at several temperatures from 440 up to 900°C was estimated using the Scherrer equation (Warren, 1990): $d_{hkl} = 0.9\lambda/(\beta \cos \theta)$, where λ is the wavelength of the X-rays and θ is the scattering angle of the (2 2 2) reflection.

Small angle X-ray scattering (SAXS) experiments were carried out using synchrotron radiation at the SAXS beamline of the Brazilian National Synchroton Light Laboratory (LNLS). Experiments were conducted with an incident wavelength $\lambda = 1.608$ Å in the range of the scattering vector q from 0.0045 to 0.17 $Å^{-1}$ (where $q = 4\pi/\lambda \ \sin(\theta)$). SAXS patterns from all the samples were collected using an imaging plate

detector and the intensity curves were corrected for parasitic scattering, integral intensity and sample absorption. Experimental data were fitted using the GNOM software (Semenyuk & Svergun 1991).

Results and discussion

Figure 1 shows thermal analysis results due to the decomposition behavior of the indium gel showing that it proceeds in three steps to form In_2O_3. The DTA curve exhibits three exothermic peaks at ~148, ~365 and ~395°C, which correlate with three steps of weight loss. The experimental weight loss up to 400°C is 70%, in agreement with the theoretical value (72.1%). The theoretical value was calculated assuming that all indium cations complexed with citric acid resulting in an indium citrate, and that during its thermal decomposition an intermediate compound was formed. This decomposition model is similar to that observed for iron and barium citrates (Srivastava et al., 1985), and proved to be suitable as shown by experimental results. In the first step of thermal decomposition (up to ~150°C) the weight loss was 35%. Since excess citric acid was added to make the gel, and due to the exothermic nature of the thermal event, the main reaction occurring in this step is related to the elimination of one molecule of free citric acid. A similar effect was observed in the decomposition of $LaMnO_{3+\delta}$ gels (Taguchi et al., 1997). In the 150–220°C temperature range, the weight loss is about 15% and is attributed to the evolution of residual nitrate, and to the decomposition of indium citrate to form an intermediate compound, as confirmed by FTIR results shown below. The last step of weight loss (from ~220 to 400°C) is characterized by the thermal decomposition of this intermediate compound to form In_2O_3. In this temperature range the DTA curve exhibits exothermic peaks around 365°C and 395°C accompanied by a weight loss of 20% due to the decomposition of organic materials in the precursor, the oxidation of free carbon being one of these reactions, and to the crystallization of indium oxide.

FTIR spectra after different thermal treatments of the gel are shown in Figure 2. The most prominent absorption bands detected after thermal annealing at 150°C are those related to (Szymanski, 1966): C=O stretching (~1728 cm^{-1}); water and COO^- group vibration (~1630 cm^{-1}); COO^- or C—O stretching (~1400 cm^{-1}); NO_3^- vibration (~1385 and 825 cm^{-1}); C—O stretching or OH deformation (~1227 cm^{-1}); C—O stretching of the organic chain (~1080 cm^{-1}), and CH_2 deformation or C—C stretching (~895 cm^{-1}). The specimen annealed at 225°C shows absorption bands due to water (~1635 cm^{-1}), COO^- vibration (~1620 and 1400 cm^{-1}), and those related to the metal–oxygen bond (~610 and 488 cm^{-1}). The FTIR spectra of samples thermally treated at higher temperatures (410–700°C) are quite similar,

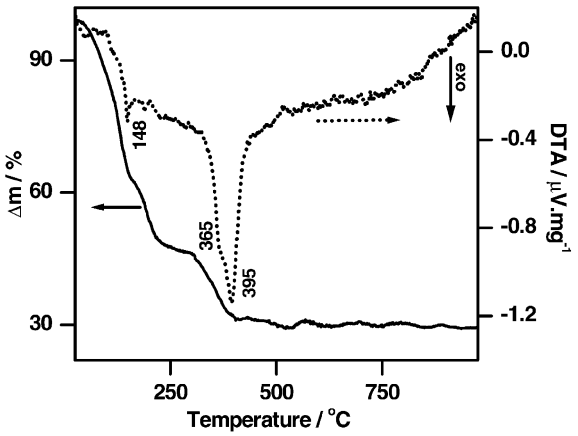

Figure 1. TG/DTA curves of the indium gel.

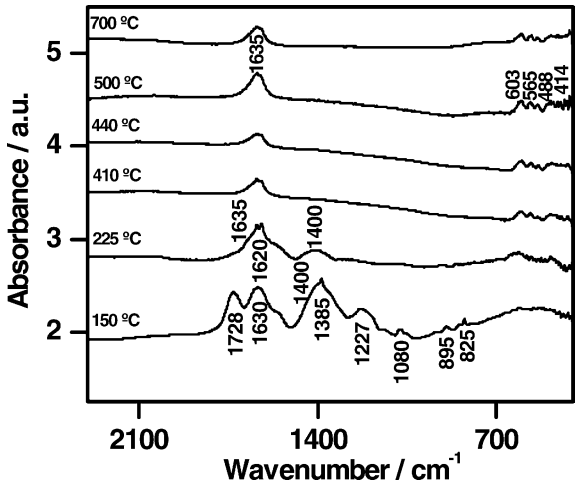

Figure 2. FTIR spectra of indium gel calcined at different temperatures for 2 h.

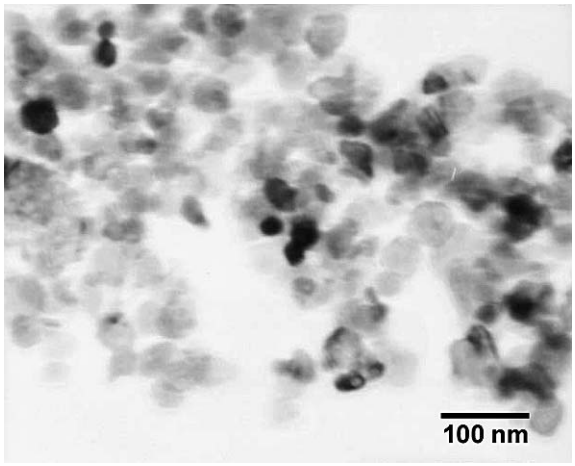

Figure 3. TEM micrograph of the In_2O_3 calcined at 500°C/2 h.

with the main absorption bands at ~1635 cm^{-1} due to water and low wavenumber bands (~603, 566, 488 and 414 cm^{-1}) which are due to the indium-oxygen bond (Nyquist & Kagel, 1971; Keller, 1986). These FTIR results corroborate those of thermal analysis.

The suggested reactions occurring during the thermal decomposition of the indium gel are summarized below, according to TG/DTA and FTIR results:

$$2InC_6H_7O_7 \cdot C_6H_8O_7 \rightarrow 2InC_6H_7O_7 + C_6H_8O_7 \qquad T < 150^\circ C$$

$$2InC_6H_7O_7 \rightarrow 2\,In(OH)\cdot(CH_2COO)_2 + 4CO/CO_2 + 2H_2O \qquad 150 \leq T \leq 220^\circ C$$

$$2In(OH)\cdot(CH_2COO)_2 \rightarrow In_2O_3 + 4CO/CO_2 + 5H_2O \qquad T > 220^\circ C$$

Figure 3 shows a representative TEM micrograph of the indium gel after calcination at 500°C for 2 h. The morphology of particles observed in the bright-field image is characterized by agglomerated nanoparticles, most of them having a spheroidal shape.

The powder X-ray diffraction pattern of the indium gel after calcination at 500°C for 30 min is shown in Figure 4a. All peaks correspond to those

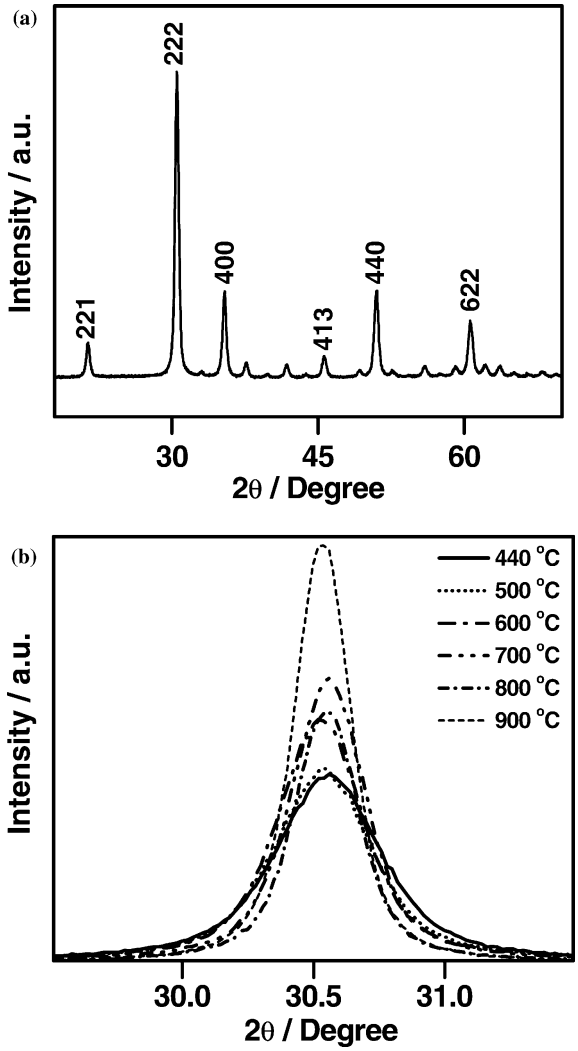

Figure 4. (a) X-ray diffraction pattern of In_2O_3 calcined at 500°C/30 min, (b) evolution of the (2 2 2) reflection with thermal treatment.

of a bixbyte type cubic structure, (space group Ia3), indexed on ICDD card 6–416, and the calculated lattice parameter is 10.072 (6) Å. The broadening of the most intense reflection (2 2 2) is seen to decrease with the calcination temperature (Figure 4b), indicating an increase in the average crystallite size. Calculation of d_{hkl} using Scherrer's equation gives values between 25 and 75 nm, indicating that the indium oxide particles prepared by this method of synthesis are in the nanosize range (<100 nm) even for calcinations at relatively high temperatures.

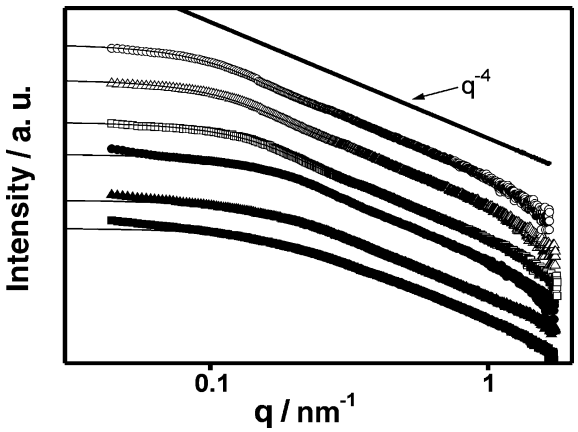

Figure 5. Scattered intensity profiles of thermally treated nanoparticles of In_2O_3. Symbols refer to experimental data of samples thermally treated at several temperatures:(■) 440; (▲)500; (●)600; (□)700; (△)800 and (○)900°C.

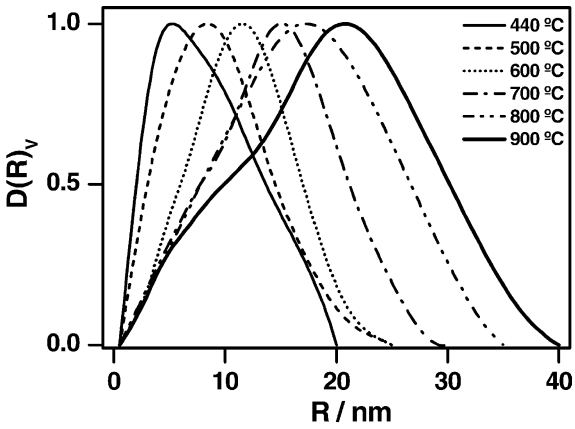

Figure 6. Volume size distribution functions calculated from the fitted experimental SAXS curves using the GNOM software.

Experimental SAXS curves versus scattering vector for powder samples calcined at several temperatures are shown in Figure 5. Results were plotted on a log–log scale, and all curves were displaced by an arbitrary factor in the intensity axis. The scattering profiles were fitted assuming a polydisperse system of spherical particles using the GNOM program. Some of the curves seem to contain the contribution of two different scattering components. One of them consists of a low-q rise and the other component is dominant in the intermediate and high-q *r*egion. The crossover between these domains depends on the calcination temperature, suggesting that the low-q scattering component is related to agglomerates of In_2O_3 nanoparticles, which increase in size with increasing the temperature of thermal treatment. For temperatures higher than 600°C the scattering by the agglomerates of indium oxide may still be present, but beyond the detection range of these experiments. In the high-q domain a power-law with an exponent of −4 is observed. This slope follows Porod's theory for high q values, indicating that the particle boundaries are sharp and smooth (Guinier & Fournet, 1955).

The program package GNOM was also used to evaluate the volumetric size distribution function $D_V(R) = (4\pi/3)R^3N(R)$, where $N(R)$ is the density of particles (functions $N(R)$ and $D_V(R)$ are given in relative units). Figure 6 displays the volumetric size distribution function calculated for all samples. These curves allow the determination of the volume weighted particle size which varies from $2R_{max} = 10$–40 nm. It can be noted that the particle size increases and the size distribution functions become broader with thermal treatment; $D_V(R)$ seems to be narrower for 440°C. There is a difference between the values of the average *crystallite* sizes obtained from XRD experiments and the *particle* size calculated from SAXS. The latter are more reliable, since they are the result of a volume weighted average, which is not the case of the Scherrer approximation.

Conclusions

An ultra-fine powder resulting from the thermal decomposition of a citrate gel precursor of In_2O_3 ceramic material was successfully prepared by a modified sol–gel technique. Results on thermal analysis and FTIR support that during the decomposition of the precursor gel an intermediate compound is formed. Calcination of this precursor material at temperatures up to 900°C gives rise to nanocrystalline particles of cubic In_2O_3 with sizes lower than 75 nm. SAXS results furnished quantitative information about dimensions and volume size distributions of the particles as a function of calcination temperature. It can also be inferred from these results that calcined materials are

composed of spherical nanoparticles with sharp and smooth surfaces.

The modified sol–gel technique used here is characterized by its remarkable simplicity, i.e. it involves no rigorous chemical procedures such as careful aging of gel and fine control of pH. Therefore, it proved to be an alternative and suitable route for the preparation of indium oxide particles in the nanosize range.

Acknowledgements

To FAPESP (95/05172-4, and 97/06152-2), CNEN and CNPq (300934/94-7) for financial support. J.F.Q. Rey acknowledges FAPESP (01/14033-0) for the scholarship. To the National Synchrotron Light Laboratory (LNLS), Campinas, Brazil, for the use of beam-time at the SAXS workstation.

References

Avivi S., Y. Mastai & A. Gedanken, 2000. Chem. Mater. 12, 1229.
Gopchandran K.G., B. Joseph, J.T. Abraham, P. Koshy & V.K. Vaidyan, 1997. Vacuum 86, 547.
Granqvist C.G., 1993. Appl. Phys. A: Solid Surf. 57, 19.
Guinier A. & G. Fournet, 1955. In: Small Angle Scattering of X-Rays. Wiley, New York.
Gurlo A., N. Barsan, U. Weimar, M. Ivanovskaya, A. Taurino & P. Siciliano, 2003. Chem. Mater. 15, 4377.
Gurlo A., M. Ivanovskaya, N. Barsan, M. Scweizer-Berberich, U. Weimar, W. Göpel & A. Diéguez, 1997. Sens. Actuat. B 44, 327.
Hamada S., Y. Kudo & T. Kobayashi, 1993. Coll. Surf. A79, 227.
Hattori T., S. Nishiyama, Y. Kishi & Y. Iwadate, 1993. J. Mater. Sci. Lett. 12, 883.
Hiroyuki Y., T. Jun, M. Koji, N. Miura & Y. Nobaru, 1997. J. Electrochem. Soc. 144, L158.
Kakihana M., 1996. J. Sol–Gel Sci. Technol. 6, 7.
Keller R.J., 1986. In: The Sigma Library of FTIR Spectra. Sigma Chemical, St. Louis, Vol. 2.
Marcilly C., P. Courty & B. Delmon, 1970. J. Am. Ceram. Soc. 53, 56.
Matsumoto, T., J. Suzuki, M. Ohnuma, Y. Kanemitsu & Y. Matsumoto, 2001. Phys. Rev. B 63, 195322.
Murali A., A. Barve, V.J. Leppert, S.H. Risbud, I.M. Kennedy & H.W.H. Lee, 2001. Nano Lett. 1, 287.
Nyquist R.A. & R.O. Kagel, 1971. In: Infrared Spectra of Inorganic Compounds. Academic Press, New York, Vol. 4.
Perez-Maquela L.A., L. Wang & E. Matijevic, 1998. Langmuir 14, 4397.
Semenyuk V., D.I. Svergun, 1991. GNOM – A program package for small angle scattering data processing. J. Appl. Cryst. 24, 537.
Srivastava A., P. Singhi, V.G. Gunjikar & A.P.B. Sinha, 1985. Thermochim. Acta 86, 77.
Steffes H., C. Imawan, F. Sozbacher & E. Obermeier, 2001. Sens. Actuat. B 78, 106.
Szymanski H.A., 1966. In: Interpreted Infrared Spectra. Plenum Press, New York, Vol. 2.
Tadashi T., S. Kengo & N. Masanori, 1993. Sens. Actuat. B 13/14, 404.
Taguchi H., S. Matsu-ura & M. Nagao, 1997. J. Solid State Chem. 129, 60.
Tahar R.B.H., T. Ban, Y. Ohya & Y. Takahashi, 1997. J. Appl. Phys. 82, 865.
Tanaka S. & T. Esaka, 2001. J. Mater. Res. 16, 1389.
Warren B.E., 1990. In: X-ray Diffraction. Dover, New York, p. 258.
Yang H., A. Tang, X. Zhang, W. Yang & G. Qiu, 2004. Scripta Mater. 50, 413.
Yura K., K.C. Fredrikson & E. Matijevic, 1990. Coll. Surf. 50, 281.
Zhan Z., W. Song & D. Jiang, 2004. J. Coll. Interface Sci. 271, 366.